Simulation of geochemical banding: Theoretical modeling and fractal structure in acidization-diffusion-precipitation dynamics

Mazen Al-Ghoul ● and Rabih Sultan ●[*]

*Department of Chemistry, American University of Beirut, Beirut, Lebanon*

In an earlier work, we presented an experimental study wherein reaction-transport processes were forged in a real rock medium. Zonation of $CaSO_4$-rich and $CaSO_4$-depleted domains were obtained and characterized. In the present study, we present a theoretical model to simulate the reaction-diffusion processes underlying the dynamics of the system. An H_2SO_4-acidization front propagating radially from a central source into a $CaCO_3$ rock bed causes dissolution of the calcite mineral and precipitation of $CaSO_4$ as either gypsum ($CaSO_4 \cdot 2H_2O$) or anhydrite (anhydrous $CaSO_4$). The deposition of $CaSO_4$ is shown to exhibit a banded texture (irregular concentric rings in two dimensions). The model involves reaction-diffusion evolution equations for three aqueous species (H^+, Ca^{2+}, and SO_4^{2-}), the $CaCO_3$ dissolution, and the deposition of $CaSO_4$, which is taken to obey a scaled Cahn-Hilliard equation. The output captures the zonation observed experimentally. Fractal analysis of the experimental contour shapes of the deposits reveals an oscillation in the fractal dimension over successive band numbers. Such oscillation is interpreted in terms of the precipitation-depletion tug scenario, not observable in regular two-dimensional Liesegang systems with high circular symmetry.

I. INTRODUCTION

In an earlier work [1], we attempted the experimental simulation of band formation in rocks, by designing a spontaneous acidization-diffusion-precipitation dynamical process in the bed of a bare rock medium, thus mimicking a possibly real natural scenario. An acidic water front was initiated at the center of a ferruginous limestone (dominantly $CaCO_3$) rock sample, via a diffusion-acidization propagation, causing the dissolution of the calcite mineral and releasing Ca^{2+}, according to the reaction

$$CaCO_3(s) + 2H^+(aq) \longrightarrow Ca^{2+}(aq) + CO_2(g) + H_2O(l). \tag{1}$$
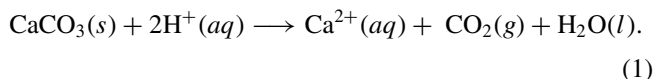
The sulfate containing water (acidified by H_2SO_4) triggers the precipitation of $CaSO_4$ (as gypsum and anhydrite minerals), by virtue of the reaction

$$Ca^{2+}(aq) + SO_4^{2-}(aq) \longrightarrow CaSO_4(s). \tag{2}$$
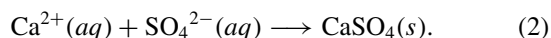
This coupled reaction-diffusion scheme was shown to yield bands of $CaSO_4$, just like in a Liesegang patterning regime [2–5]. The zonation obtained in this attempt (the detailed procedure is described in Ref. [1]) is depicted in Fig. 1.

In the present study, we propose a theoretical scheme incorporating reduced forms of reactions 1 and 2, coupled to the diffusion of H^+ and SO_4^{2-}, to model the dynamical processes leading to the pattern formation. Subsequently, we analyze the textural and topological aspects of the band contours, from the viewpoint of fractal structure.

Theory background

Interest in modeling geochemical dynamical processes started growing since the early 1980s [6], when the need for such a theoretical framework became a necessity for the understanding of a broad class of natural phenomena. Although our study focuses on the beautiful periodicity, often manifested as colorful band alternations in a wide variety of rocks and notably in agates, dynamic processes in geophysics and geochemistry are not limited to this widely spread scenery. They extend over the various aspects of environmental changes in the complex geospace surrounding our planet, and their formulation has become indispensable, notably in facing the intricate problems of climate change. Thus earthquakes, floods, winds, atmospheric pollution, coastal alterations, and topographical and tectonic deformations have all necessitated a relatively new approach, involving *nonlinear* dynamical formulation. Many such processes obey power laws [7], and are described by nonlinear differential equations.

Banding in rocks has commonly been associated with the Liesegang phenomenon [8,9] of rhythmic precipitation in gels. Two principal processes taking place on widely different time scales, namely a fast precipitation reaction, coupled to slow diffusion of coprecipitate ions generate a pattern of parallel precipitate bands, coined a "Liesegang pattern" since its observation by Liesegang in 1896 [2–4]. This striking similarity has inevitably led to a similitude in the model equations describing the formation of the Liesegang bands on one hand, and the geochemical bands on the other. Once it is formed, a Liesegang pattern is spatially "locked" in the gel, just like the mineral bands persist in the rock bed for very long times (millions of years). A survey of geochemical self-patterning phenomena and geochemistry-Liesegang analogy studies in literature reviews and special edited volumes is found in Refs. [6,10–13].
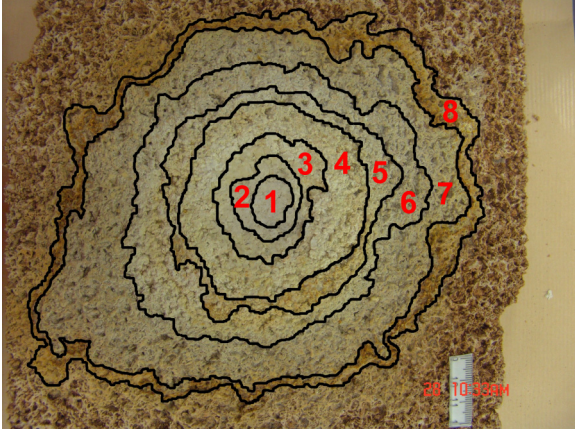
[*]rsultan@aub.edu.lb

FIG. 1. Ferruginous limestone rock infiltrated by an H_2SO_4-acidulated water from the center, outwards. Zonation inside the rock is marked by an alternation of $CaSO_4$-rich and $CaSO_4$-depleted domains. The experiment is described in Ref. [1]. The rock piece is 25 cm (length) $\times$ 23 cm (width) $\times$ 3 cm (height or depth).

Mathematical modeling in geomorphological dynamics, shear-flow mechanisms, melt pressure deformations, rheological flow, and metamorphism has witnessed growing importance in the last four decades, notably in unraveling the complex scenarios underlying the physicochemical phenomena involved in architecting the emerging relief and geographical landscape. The dynamical description (equations) encompasses the flow and percolation of underground water, heat transfer processes, mass transfer, and last but not least (of particular relevance in the present study), chemical reactions. Phillips established that self-organization dynamical theories have profound implications on the nature and trajectories of landscape evolution and earth-surface system behavior [14]. He advanced a theory of spatially divergent self-organization wherein autogenic differentiation is proved to be directly linked to dynamical instability and chaos. A review of mathematical models and analytical methods describing basin-scale hydrogeologic transport processes, with applications to specific, world-spread sedimentary basins, is presented by Person *et al.* [15]. Nonequilibrium actively deforming orogenetic belts may generate dissipative structures by self-organization [16]. The modeling of melt pressure buildup helps in the interpretation of crustal-scale shear-zone and fracturing systems [16]. An overview of the methodologies for the simulation of fractured porous media based on the evaluation of excluded volume, continuum percolation, and power laws is found in Ref. [17]. Physical models for the seismic cycle were developed [18] to provide alarming tools for upcoming earthquakes.

In his monograph [19], Ortoleva demonstrates that geochemical self-organization is possible in all types of rocks: sedimentary, metamorphic, and igneous. Omnipresent noise and small local perturbations can be amplified to unfold into dissipative structures, yielding patterns of all symmetries and spanning widely different length scales.

Geochemical banding is not always a result of a self-patterning "template." Sedimentary layering is merely formed by seasonal variations, attributed to causes external to the rock system [19,20]. Yet, self-organization mechanisms mediated
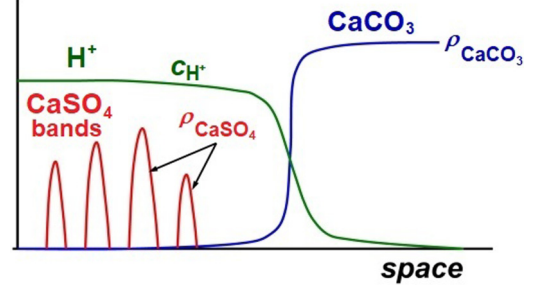

FIG. 2. Acid infiltration front (H^+) causing the dissolution of the main rock mineral ($CaCO_3$). Another mineral ($CaSO_4$) undergoes a banded deposition behind the dissolution front.
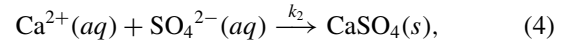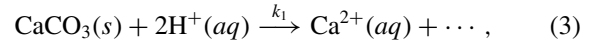
by nonequilibrium instabilities within the rock medium were thoroughly investigated and demonstrated in a variety of studies [19–29].

II. MODELING GEOCHEMICAL SELF-ORGANIZATION

A. Model equations

In this subsection, we present a model of geochemical banding, incorporating the diffusion of H^+ and SO_4^{2-} from a central reservoir coupled to the reactions of dissolution of $CaCO_3$ [Eq. (1)] and precipitation of $CaSO_4$ [Eq. (2)].

Equations (1) and (2) describing the chemistry that takes place in the system are further simplified to the reduced scheme:

$$CaCO_3(s) + 2H^+(aq) \xrightarrow{k_1} Ca^{2+}(aq) + \cdots, \qquad (3)$$

$$Ca^{2+}(aq) + SO_4^{2-}(aq) \xrightarrow{k_2} CaSO_4(s), \qquad (4)$$

where k_1 and k_2 are the rate constants for the dissolution of $CaCO_3$ in acid and the precipitation of $CaSO_4$, respectively. We anticipate the precipitation of $CaSO_4$ behind the $CaCO_3$ dissolution front, depicted in Fig. 2 for a one-dimensional (1D) spatial propagation. Such a scheme was predicted and demonstrated [30] for the deposition of the goethite mineral, behind a pyrite dissolution front.

The system can then be modeled using the following set of reaction-diffusion equations [31]:

$$\frac{\partial c_{H^+}}{\partial t} = D_{H^+}\nabla^2 c_{H^+} - 2k_1 c_{H^+}^2 \rho_{CaCO_3}, \qquad (5)$$

$$\frac{\partial c_{Ca^{2+}}}{\partial t} = D_{Ca^{2+}}\nabla^2 c_{Ca^{2+}} + k_1 c_{H^+}^2 \rho_{CaCO_3} - k_2 c_{Ca^{2+}} c_{SO_4^{2-}}, \qquad (6)$$

$$\frac{\partial c_{SO_4^{2-}}}{\partial t} = D_{SO_4^{2-}}\nabla^2 c_{SO_4^{2-}} - k_2 c_{Ca^{2+}} c_{SO_4^{2-}}, \qquad (7)$$

$$\frac{\partial \rho_{CaCO_3}}{\partial t} = D_{CaCO_3}\nabla^2 \rho_{CaCO_3} - k_1 c_{H^+}^2 \rho_{CaCO_3}, \qquad (8)$$

where c_i, ρ_i, and D_i represent the concentration, number density (for solids), and diffusion coefficient of the ith species. These reaction-diffusion equations in principle model a
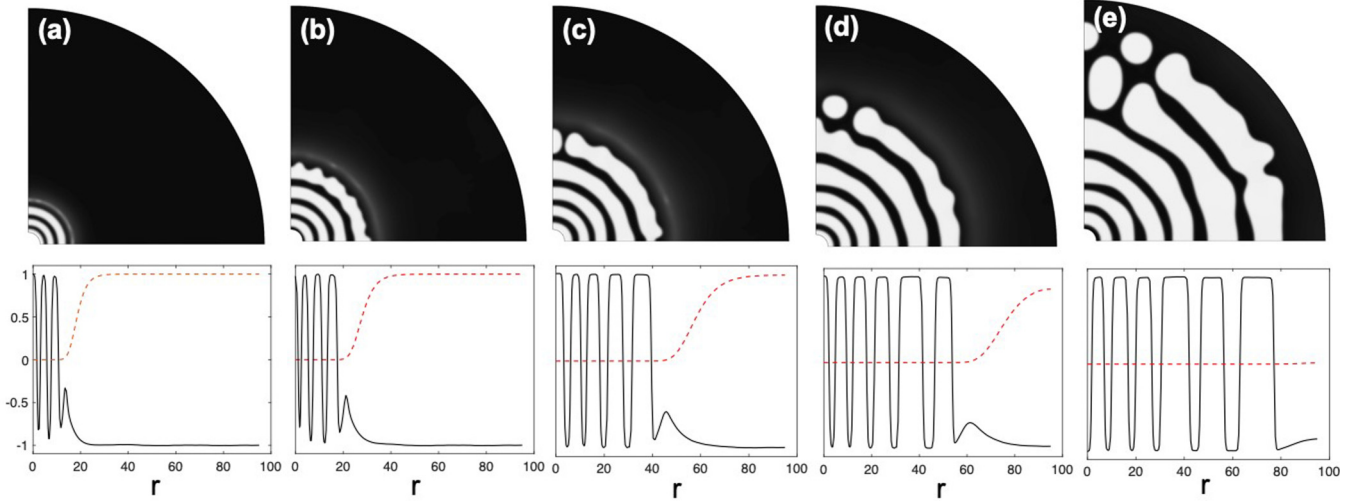
FIG. 3. Upper panels: Time evolution of the simulated gypsum banding pattern (ϕ): (a) $t = 14$, (b) $t = 20$, (c) $t = 140$, (d) $t = 250$, (e) $t = 600$. Lower panels: Evolution of the bands via a one-dimensional cut of the patterns above along a diagonal radius r (solid line) and of the dissolution of calcium carbonate ρ_{CaCO_3} (dashed line). Model parameters: $k_1 = k_2 = 1$; $D_{H^+} = 10$, $D_{Ca^{2+}} = 2$, $D_{SO_4^{2-}} = 2$, $D_{CaCO_3} = 1$; $\sigma = 0.1$, $\lambda = 1$.

moving dissolution front which generates a homogeneous colloidal cluster of $CaSO_4$ in its wake. When its local concentration attains a certain critical value, $CaSO_4$ segregates into regions of high concentrations $\rho_{CaSO_4}^h$ (precipitate) and low concentrations $\rho_{CaSO_4}^l$ (no precipitate) via a spinodal decomposition scenario, which is described by a Cahn-Hilliard equation [32,33]. This mixing of reaction-diffusion processes with a spinodal decomposition setting for precipitate formation was proposed by Antal *et al.* [32] to explain Liesegang banding in precipitate systems. In this model, the periodic precipitate pattern emerges from a spinodal decomposition of colloidal reaction products in the wake of a moving reaction front. It provides an alternative view to those that invoke nucleation and growth models (such as those used to generate Fig. 2), and this in fact results in evolution equations that are simpler to solve numerically and yield very good agreement with experiments, especially those related to the spacing, width, and time laws encountered in the classical Liesegang systems [32]. Subsequently, many theoretical studies that are constructed on such a prototype have followed; for example, to model the transition from bands to spots in the cadmium hydroxide and cadmium sulfide precipitation systems [33] and to describe the effect of noise on helical patterns [34]. We hereby couple the evolution equations (5)–(8) to the following Cahn-Hilliard equation describing the formation of the precipitate $CaSO_4$:

$$\frac{\partial \phi}{\partial t} = -\lambda \nabla^2 (\sigma \nabla^2 \phi + \phi - \phi^3) + k_2 c_{Ca^{2+}} c_{SO_4^{2-}}, \quad (9)$$

where $\phi = (\rho_{CaSO_4} - \bar{\rho}_{CaSO_4})/\hat{\rho}_{CaSO_4}$ represents the precipitation field that is shifted by $\bar{\rho}_{CaSO_4} = (\rho_{CaSO_4}^h + \rho_{CaSO_4}^l)/2$ and scaled by $\hat{\rho}_{CaSO_4} = (\rho_{CaSO_4}^h - \rho_{CaSO_4}^l)/2$ so that its value ranges between -1 (no precipitate) and $+1$ (precipitate). The parameters λ and σ are the rescaled kinetic coefficient and surface tension, respectively. The ratio σ/λ defines a characteristic time scale of the growth of unstable modes in precipitation.

B. Method and results

We consider solving the evolution equations (5)–(9) inside the domain Ω that consists of an outer quarter circle of radius $r_{out} = 100$ and an inner radius (the reservoir) of radius $r_{in} = 5$. The initial conditions inside Ω for c_{H^+}, $c_{Ca^{2+}}$, $c_{SO_4^{2-}}$, ρ_{CaCO_3}, and ϕ are chosen such that $c_{H^+}(t = 0) = c_{Ca^{2+}}(t = 0) = c_{SO_4^{2-}}(t = 0) = 0$, $\rho_{CaCO_3}(t = 0) = 1$, and $\phi(t = 0) = -1$, all perturbed with 1% Gaussian noise. The boundary conditions are chosen such that c_{H^+} is fixed at the inner circular boundary, and no-flux boundary conditions for all the species along the outer circular boundary are applied. Equations (5)–(9) are solved numerically using a vertex-based finite volume method on unstructured meshes, whereby the spatial discretization is carried out using the control volume finite element method (CVFEM). The resulting nonlinear differential equations are successfully integrated using a fast and robust scheme based on operator splitting and a line search Jacobian-free Newton-Krylov method [35]. The structureless mesh, which is generated by the open source software TRIANGLE, is suitable to reproduce the complex geometry of Ω. The time evolution of the banding of gypsum is represented by the field ϕ as depicted in Fig. 3 and in the movie in the Supplemental Material [36].
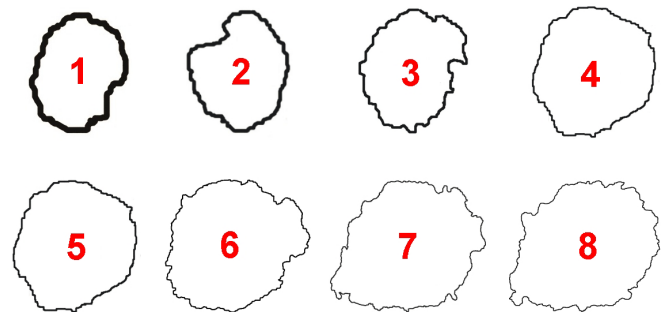

FIG. 4. Outer contours of the various zones of the acidified rock shown in Fig. 1.
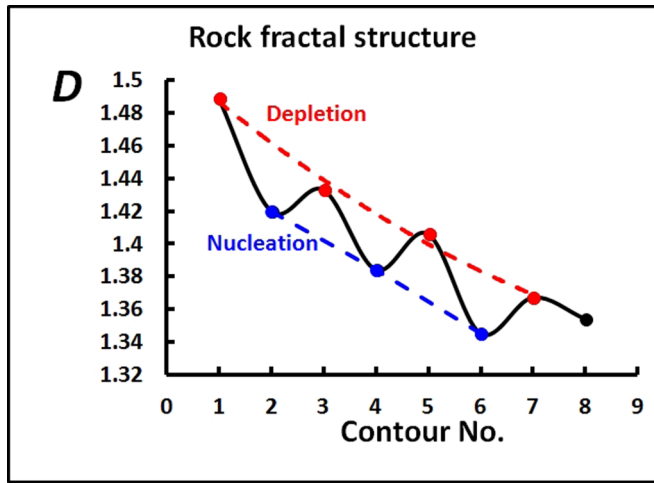
FIG. 5. Variation of the fractal dimension with contour number from the inner to outer regions. The alternation seems to be correlated with the process delineating the contour, i.e., precipitation (troughs) vs depletion (peaks).
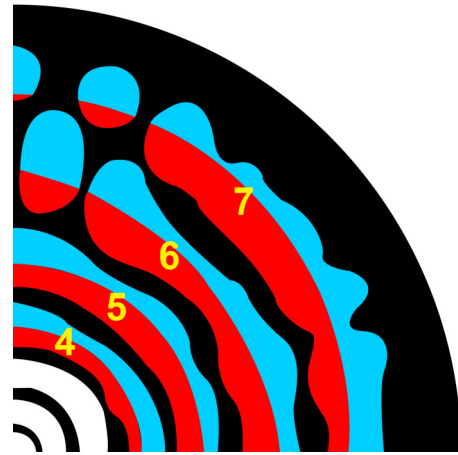

FIG. 6. Band contours similar to the ones in Fig. 4, but here obtained theoretically by the computations of Sec. II. In each band, the red portion represents the band tail (back), while the blue portion describes the band head (front).

The features of the bands are elucidated by a one-dimensional radial cut through the two-dimensional patterns, clearly showing congruence with the well-known empirical laws of Liesegang banding. These are verified by an increasing spacing (often referred to as direct spacing) and an increasing bandwidth as a function of the radius r (see lower panels in Fig. 3). The bands start growing in the wake of the dissolution front of calcium carbonate (the dashed curves in Fig. 3), due to the invading acid which in turn generates the calcium ions via reaction 1. It is also important to note that the model accounts for the wiggle structure in the band contours, i.e., the departure from circularity, as observed in the experiments [1]. The introduced noise perturbation captures the randomness in the contour shapes in lieu of percolation, as rock porosity effects were not considered here.

The present method is a distinct variant from our work on Liesegang patterns with redissolution in the absence [37] and presence [38] of an electric field, using the model of Müller and Polezhaev [39].

III. FRACTAL REACTION FRONT CONTOURS

We now focus on the shape of the front contours in the different regions. The shape of the acidization front is to a large extent governed by porosity variations [40,41]. As a result, irregularities emerge, and thus may give rise to fractal structures. After choosing a specific region (from domains 1 to 8; see Fig. 1), the RGB (Red-Green-Blue) image is cropped, and its outer contour is retained, as seen in Fig. 4.

The contour image is then transformed to black and white and analyzed using the FRACTALYSE and FRAC3E software. The results agree within 5–7%, but the qualitative trend in moving from contour 1 to contour 8 is similarly and almost exactly reproduced.

We characterize each contour by its fractal dimension D, which is the slope of the linear plot of $\ln n(\xi)$ versus $\ln(1/\xi)$, where $n(\xi)$ is the contour coverage, and ξ is the varied length scale. D is determined here by the box count

method [7,42]. The values of the fractal dimension D and its variation throughout the regions are plotted in Fig. 5.

The outcome is quite interesting, as we remark that D oscillates in going from one contour to the next one. This oscillation can be understood on the following basis. We distinguish between two types of contours: depletion contours defining the edge of a zone rich in $CaSO_4$ (contours 1, 3, 5, and 7 in Fig. 1), and precipitation contours which mark the onset of the formation of a new band beyond an interband zone (contours 2, 4, 6, and 8 in Fig. 1). The peaks correspond to depletion contours while the troughs represent the precipitation ones. When a band starts forming, the delineated contour will eventually have a lower fractal dimension than the outer edge of the preceding one; and when the medium is depleted marking the ending edge of the newly formed band, the fractal dimension increases. In other terms, the head contour of a $CaSO_4$-rich band will always have a higher D than its tail contour.
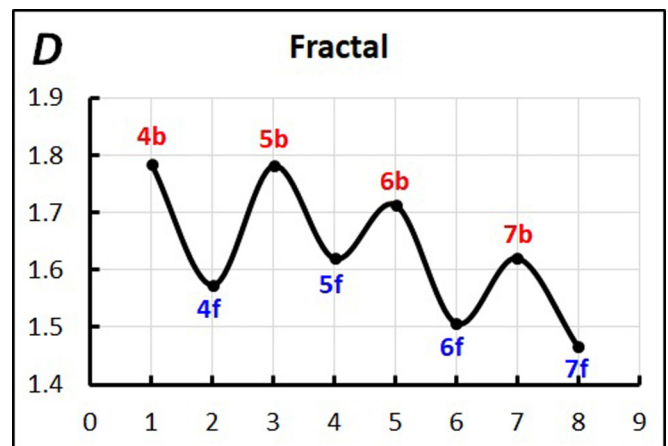

FIG. 7. Fractal dimensions of the back (b) and the front (f) of the conjectured bands of Fig. 6. The oscillations capture the experimental oscillations and the decreasing trend seen in Fig. 5.

In parallel to this experimental fractal analysis, we now consider the fractal contours in the bands simulated in Sec. II. We consider the final pattern and distinguish between the fractal structure of the back contours (red) and the front ones (blue), as depicted in Fig. 6. The back and the front portions of a given band are analyzed for fractal structure, each separately. The fractal dimension is computed by the box-count method, and the results are plotted in Fig. 7.

We see that the oscillations in the fractal dimension of the conjectured contours strikingly capture the features of the experimental ones. The maxima and the minima appear to be in harmony with those of Fig. 5. The essentially decreasing strength in the fractal dimension is also reproduced.

IV. CONCLUSIONS

This work complements the *in situ* experimental work of Ref. [1]. A model of nonlinear reaction-diffusion equations coupled to a Cahn-Hilliard-type precipitation scheme for $CaSO_4$ captured the formation of $CaSO_4$ Liesegang bands. The band contours exhibited wiggled structures, instead of the traditional circular shapes obtained in a normal gel experiment. Oscillations in the fractal dimension from one contour to the next one suggest a bifractal nature, which seems to be correlated with the depletion-precipitation scenario in the gypsum mineral. The theoretical oscillations are in good agreement with the ones obtained experimentally.

[1] M. Msharrafieh, M. Al-Ghoul, F. Zaknoun, H. El-Rassy, S. El-Joubeily, and R. Sultan, Chem. Geol. **440**, 42 (2016).

[2] R. E. Liesegang, Chem. Fernwirkung, Lieseg. Photograph. Arch. **37**, 305; **37**, 331 (1896).

[3] E. S. Hedges, *Liesegang Rings and Other Periodic Structures* (Chapman and Hall, London, UK, 1932).

[4] H. K. Henisch, *Crystals in Gels and Liesegang Rings* (Cambridge University Press, Cambridge, UK, 1988).

[5] Wi. Ostwald, Lehrbuch Allg. Chem. **2**. Aufl., Band 2, 2. Teil: Verwandtschaftslehre, Engelmann: Leipzig, 1896-1902, p. 778.

[6] S. LoveJoy, F. Agterberg, A. Carsteanu, Q. Cheng, J. Davidsen, H. Gaonac'h, V. Gupta, I. L'Heureux, W. Liu, S. W. Morris, S. Sharma, R. Shcherbakov, A. Tarquis, D. Turcotte, and V. Uritsky, EOS **90**, 455 (2009).

[7] M. Schroeder, *Fractals, Chaos, Power Laws, Minutes from an Infinite Paradise* (Dover, New York, 2009).

[8] R. E. Liesegang, *Geologische Diffusionen* (Steinkopff, Dresden, 1913); *Die Achate* (Steinkopf, Dresden-Leipsig, 1915).

[9] R. Sultan and A. Abdel-Rahman, Lat. Am. J. Solids. Struct. (LAJSS) **10**, 59 (2013).

[10] E. Merino, in *Chemical Instabilities*, NATO-ASI Series Vol. 120 (Springer, Berlin, 1984), pp. 305–328.

[11] S. Sadek and R. Sultan, in *Precipitation Patterns in Reaction-Diffusion Systems*, edited by I. Lagzi (Research Signpost, Trivandrum, 2011), Chap. 1, pp. 1–43.

[12] *Growth, Dissolution and Pattern Formation in Geosystems*, edited by B. Jamtveit and P. Meakin (Kluwer, Dordrecht, 1999).

[13] *Fractals and Dynamic Systems in Geoscience*, edited by J. H. Kruhl (Springer-Verlag, Berlin, 1994).

[14] J. D. Phillips, Ann. Assoc. Am. Geogr. **89**, 466 (1999).

[15] M. Person, J. P. Raffensperger, Sh. Ge, and G. Garven, Rev. Geophys. **34**, 61 (1996).

[16] M. Brown and G. S. Solar, J. Struct. Geol. **20**, 211 (1998).

[17] P. M. Adler, J. F. Thovert, and V. V. Mourzenko, *Fractured Porous Media* (Oxford University Press, Oxford, UK, 2013).

[18] G. Zöller, M. Holschneider, and J. Kürths, in *Analysis and Control of Complex Nonlinear Processes in Physics, Chemistry and Biology*, edited by L. Schimansky-Geier, B. Fiedler, J. Kurths, and E. Schöll (World Scientific, Singapore, 2007).

[19] P. Ortoleva, *Geochemical Self-Organization* (Oxford University Press, New York, 1994).

[20] E. Merino and Y. Wang, in *Non-Equilibrium Processes and Dissipative Structures in Geoscience*, Year-Book for Complexity in Natural, Social, and Human Sciences Vol. 11, edited by H.-J. Krug and J. H. Kruhl (Duncker and Humblot, Berlin, 2001), pp. 13–45.

[21] P. Ortoleva, J. Chadam, E. Merino, and A. Sen, Am. J. Sci. **287**, 1008 (1987).

[22] P. Ortoleva, E. Merino, C. Moore, and J. Chadam, Am. J. Sci. **287**, 979 (1987).

[23] Y. Wang, M. A. Chan, and E. Merino, Sci. Rep. **5**, 10792 (2015).

[24] Y. Wang and E. Merino, Geochim. Cosmochim. Acta **56**, 587 (1992).

[25] A. E. Boudreau, Mineral. Petrol. **54**, 55 (1995).

[26] B. P. Boudreau, *Diagenetic Models and Their Implementation: Modeling Transport and Reactions in Aquatic Sediments* (Springer, Berlin, 1997).

[27] A. D. Fowler and I. L'Heureux, Can. Mineral. **34**, 1211 (1996).

[28] I. L'Heureux, Philos. Trans. R. Soc. A **371**, 20120356 (2013).

[29] M. Chacron and I. L'Heureux, Phys. Lett. A **263**, 70 (1999).

[30] R. Sultan, P. Ortoleva, F. De Pasquale, and P. Tartaglia, Earth-Sci. Rev. **29**, 163 (1990).

[31] B. C. Eu and M. Al-Ghoul, *Chemical Thermodynamics: Reversible and Irreversible Thermodynamics*, 2nd ed. (World Scientific, Singapore, 2018).

[32] T. Antal, M. Droz, J. Magnin, and Z. Rácz, Phys. Rev. Lett. **83**, 2880 (1999); T. Antal, M. Droz, J. Magnin, Z. Rácz, and M. Zrinyi, J. Chem. Phys. **109**, 9479 (1998).

[33] M. Dayeh, M. Ammar, and M. Al-Ghoul, RSC Adv. **4**, 60034 (2014).

[34] S. Thomas, I. Lagzi, F. Molnár, and Z. Rácz, Phys. Rev. Lett. **110**, 078303 (2013).

[35] A. Abi Mansour and M. Al-Ghoul, Phys. Rev. E **89**, 033303 (2014).

[36] See Supplemental Material at http://link.aps.org/supplemental/10.1103/PhysRevE.100.052214 for a movie showing the time evolution of the banding of gypsum.

[37] M. Al-Ghoul and R. Sultan, J. Phys. Chem. A **105**, 8053 (2001).

[38] M. Al-Ghoul and R. Sultan, J. Phys. Chem. A **107**, 1095 (2003).

[39] S. C. Müller and A. A. Polezhaev, Chaos **4**, 631 (1994).

[40] K. Lund, H. S. Fogler, and C. C. McCune, Chem. Eng. Sci. **28**, 691 (1973).

[41] K. Lund and H. S. Fogler, Chem. Eng. Sci. **31**, 373 (1976).

[42] T. Vicsek, *Fractal Growth Phenomena*, 2nd ed. (World Scientific, Singapore, 1992).